Simulation of a High Reynolds Number Compressible Turbulent Boundary Layer Developing in the Presence of a Sinusoidal Plane

Jonathan J. Gaskins*, Jonathan Poggie†, and Gregory Blaisdell‡
Purdue University, West Lafayette, Indiana, 47907-2045, USA

In the development of high-speed aerodynamic applications, it is necessary to consider how imperfect conditions can affect the dynamics of a system. This study aims to continue investigations into how a roughened surface will affect the behavior of a compressible turbulent boundary layer. Visualizations of the flow have shown the presence of near-wall streaks of high and low-speed fluid which have been a well documented coherent structure of turbulent boundary layers. Observations of the streaks in the rough wall cases show that the scale of their structure is small enough to allow navigation around the roughness elements. We suggest this may be a physical description of the mechanism responsible for the Reynolds number similarity hypothesis. Investigations into the skin friction of the surface have shown differences between the smooth and rough cases. The rough cases have shown significant large areas of high C_f which convect downstream and are affected by the presence of the roughness elements. The generation of turbulence kinetic energy was found to increase just past the peak of the roughness elements and become negative in the forward-facing portion of the roughness elements. This is consistent with what is observed regarding the pressure gradients along the surface. A direct calculation method was used to determine the effective C_f used for scaling of variables. This method proved particularly effective in analyzing a rough wall turbulent boundary layer due to the determination of the primary drag force on the surface which characterizes rough flow regimes.

Nomenclature

C_f	=	skin friction coefficient
C_{fe}	=	effective skin friction coefficient
ES	=	effective slope
k	=	roughness height
k_s	=	equivalent sand grain roughness height
P	=	production of turbulence kinetic energy
TKE	=	turbulence kinetic energy
u^+_{VD}	=	Van Driest transformed inner-scaled velocity
u_τ	=	friction velocity
Δu^+	=	roughness function
κ	=	von Karman constant
τ_w	=	wall shear stress
Ξ	=	diagnostic function

I. Introduction

In the design of high-speed flow systems, it is useful to know how imperfections (inherent or induced) of the designed geometry will affect the flow interacting with the surface. Roughness is an imperfection which can be seen in a wide variety of applications, including pitting on turbine blades, ice accretion on aircraft wings, and under the atmospheric boundary layer buildings and trees can be considered roughness [1]. Studying roughness has practical

*Graduate Research Assistant, School of Aeronautics and Astronautics, gaskinsj@purdue.edu
†Professor, School of Aeronautics and Astronautics, jpoggie@purdue.edu, AIAA Associate Fellow.
‡Professor, School of Aeronautics and Astronautics, blaisdel@purdue.edu, AIAA Associate Fellow

applications, since the nonuniform surface can affect the turbulence generation near the surface, and thus the transfer of heat and momentum across the boundary layer. This can affect heating of the surface and the performance of the system in use. In high speed applications where heating is of particular interest, it is important to know how a rough topology may affect the localized heating of the surface from shear stress forces and viscous dissipation of kinetic energy. Many studies [1] investigating roughness have been performed in the incompressible regime, but there have been far fewer studies in the high-speed compressible regime. The objective of this study is to investigate how a compressible turbulent boundary layer behaves in the presence of a sinusoidal surface, emulating a surface with geometric imperfections.

A. The Flat-Plate Turbulent Boundary Layer

To determine how the presence of geometric imperfections will affect a turbulent boundary layer, it is useful to start with the ideal flat-plate turbulent boundary layer as a baseline. The scaling and structure of a flat-plate turbulent boundary layer is well documented and is briefly discussed here.

1. Scaling of an Incompressible Turbulent Boundary Layer

When considering scaling of the incompressible turbulent boundary layer, it is important to note that different parameters have different significance depending on the location of interest through the boundary layer. Near the wall, parameters are typically described in inner units where the friction velocity, calculated as $u_\tau = \sqrt{\frac{\tau_w}{\rho}}$, is the velocity scale, and the viscous length scale is determined from ν/u_τ. Parameters scaled in the inner region are denoted with a "+" superscript. The outer region of the boundary layer acts like a wake of the boundary layer further upstream. For this reason the velocity is discussed in terms of the defect velocity. The parameters typically used to discuss the outer region of the boundary layer is the inner-scaled defect velocity ($\bar{u}_D^+$), and the wall-normal location scaled by the boundary layer thickness (y/δ). We define δ to be the location where the velocity is $u = 0.99U_\infty$.

2. Structure of the Turbulent Boundary Layer

The variation of wall-bounded flows from the no-slip condition at the wall to the freestream conditions far from the wall shows that the flow characteristics can change greatly dependent on the wall-normal location (defined as y in this study, with x and z being the streamwise and spanwise directions, respectively.). As the wall-normal location is changed, there are regions where different characteristics of the flow can be used to define a region.

If dimensional analysis is utilized on the region near the wall, it can be shown that the inner-scaled velocity is a function of the inner-scaled wall-normal location, or

$$u^+ = f(y^+). \tag{1}$$

This is referred to as the law of the wall. It can be shown that very near the wall, the inner-scaled velocity is given by

$$u^+ = y^+. \tag{2}$$

This is typically valid for $y^+ < 5$ and its region is referred to as the viscous sublayer or sometimes the linear sublayer. In this region, turbulence fluctuations are negligible and viscous forces are dominant.

If dimensional analysis is used on the outer region of the turbulent boundary layer, we can find that

$$\bar{u}_D^+ = g\left(\frac{y}{\delta}\right). \tag{3}$$

The outer region behaves like a wake of the boundary layer further upstream. It is convenient to discuss the velocity in terms of a defect velocity (u_D). The outer region is typically defined as $y^+ > 50$.

For high Reynolds number flows, there is an overlap region where Equation 1 and Equation 3 are both valid. If an analysis is carried out where the inner and outer forms of velocity are valid, the inner-scaled velocity is found to have a logarithmic variation. The inner-scaled velocity in this region is

$$u^+ = \frac{1}{\kappa}\log y^+ + B, \tag{4}$$

where κ is the von Karman constant (≈ 0.41) and B is an additive constant (≈ 5.2). The logarithmic region lies between $y^+ > 50$ and $y/\delta < 0.3$. This is an important region as there is a general consensus that a sufficiently developed flow with high enough Reynolds number will have a logarithmic region that is reasonably defined by Equation 4.

The region where $5 < y^+ < 50$ is called the buffer layer, and is characterized by a transition of viscous dominanted flow, to flow where the Reynolds stresses are more significant. The viscous sublayer, buffer layer, and logarithmic region are of typical interest in this study, because the presence of roughness elements can directly disturb these layers. These layers are significant regions in regards to the production of turbulence kinetic energy (TKE). Though the outer layer may not be directly affected, it is possible that nonlinear disturbances can propogate to the outer region of the boundary layer (which encompasses most of the boundary layer).

The identification of different regions in a turbulent boundary layer is advantageous because it gives some order to a rather chaotic nonlinear process and these regions are found in most turbulent boundary layers. Similarly, the search for coherent structures in turbulence is attractive because it can introduce the idea that there may be patterns which are common to different turbulent flows. Coherent structures can give information about dominant mechanisms of momentum and energy transfer which can be of practical interest.

Of particular interest to this study is the presence of low and high-speed streaks of flow where the wall-normal location is $y^+ \approx 10$. These streaks are associated with pairs quasi-streamwise vortices (which can become the legs of hairpin vortices), that induce a flow upwards of low momentum fluid from the wall, which causes a region of low-speed flow between the vortices [2]. These vortices can join to form a head of a hairpin vortex, which can convect downstream and grow to interact with the outer region of the boundary layer. In both the formation of hairpin vortices (which have been observed in the outer region of the boundary layer), and in the induced wall-normal velocity of low momentum fluid (and by extension the flow of high-speed fluid towards the wall), a disruption of these streaks could affect the large-scale characteristics of the boundary layer.

3. Scaling of a Compressible Turbulent Boundary Layer

For compressible turbulent boundary layers, the effect of varying density must be accounted for. The Van Driest transformation [3] is often used to transform velocity of adiabatic flows. The Van Driest transformation is given by

$$u^+_{VD} = \int_0^{u^+} (\overline{\rho}/\rho_w)^{1/2}\, du^+ \tag{5}$$

where $\overline{\rho}$ is the mean density as a function of y, and ρ_w is the density at the wall. Scaling of Reynolds stresses can be accomplished using Morkovin scaling [4] which creates a modified friction velocity. Morkovin's hypothesis is that compressibility effects on turbulence fluctuations are only important for high Mach number boundary layer flows (M>5) or supersonic free shear flows (M>1.5). The modified value of the friction velocity can be found by scaling using local mean density

$$\sqrt{\frac{\overline{\rho}_w}{\overline{\rho}}}u_\tau. \tag{6}$$

Studies from Zhang et al. [5] have outlined semi-local scaling methods, where scaling parameters are quantified as functions of wall-normal location. This will be investigated as a scaling method in future work.

B. Roughness Effects on a Turbulent Boundary Layer

Some of the earliest investigations into rough-wall turbulent flows were performed by Nikuradse [6] with pipes coated in sand. Subsequent work from Colebrook [7] and Moody [8] built upon Nikuradse's work. As a consequence, a common way to classify rough surfaces is by using the equivalent sand grain roughness height (k_s). If the surface roughness is very comparable to the original sand grain roughness of Nikuradse's experiments, then k_s will be equivalently k (the roughness height). To determine the equivalent k_s for a surface which differs from the original sand experiments, a hydrodynamic test is needed in the fully rough regime [9].

There are different regimes of rough-wall flows. These are dependent upon the magnitude of the disturbance of the roughness elements to the structure of the boundary layer. Hydraulically smooth flow maintains the presence of the viscous sublayer. Transitionally rough flow, which can have varying effects, shows that viscous forces on the surface and form drag on the roughness elements are both important to the flow. Fully rough flow shows the destruction of the viscous sublayer and form drag on the roughness elements is the primary drag force [1]. These regimes can be defined by the inner scaled equivalent sand grain roughness height (k_s^+). The threshold for the fully rough regime is defined as $k_s^+ > 70$. The direct effect of roughness can usually be observed for $y < 5k_s$ [10].

A primary effect of roughness that has been observed in incompressible flows is the presence of the roughness function (Δu^+). This is a value which is subtracted from the inner-scaled log-law, representing an increase in skin friction from the roughness elements. This has been observed in incompressible and compressible studies.

Turbulence is a highly nonlinear process, and a valid question is if the effects near the wall can have a cascading effect to the outer region of the boundary layer. Townsend's Reynolds number similarity hypothesis [11] (and its extension from Perry and Chong [12] and Raupach et al. [13]) states that at sufficiently large Reynolds number, the length scales near the wall and far from the wall are disparate enough that the large scale motions will remain unchanged, and the boundary layer will be unchanged with the exception of a modified friction velocity, a modified boundary layer thickness, and a region near the roughness known as the roughness sublayer. This is represented by observing similar shapes of profiles to the baseline case above the roughness sublayer. In the case of velocity, this can be seen by plotting defect velocities. Flack and Schultz [9]have found this hypothesis to be widely applicable to a variety of rough surfaces and Reynolds numbers in incompressible flows.

In compressible turbulent boundary layer experiments, Bowersox and Latin [14] [15] found that roughness elements can protrude into the supersonic region of the boundary layer and cause shock waves and expansion fans around the roughness elements. This could point to significant variations across the boundary layer as compared to incompressible flows. A study from Ekoto et al. [16, 17] found that the Reynolds stresses increased at the forward portion of the roughness elements and decreased in the aft portion. Peltier et al. [18] found that the Reynold stresses and inner-scaled mean velocity profiles were lower in magnitude than the smooth wall case.

The objective of this study is to investigate how a roughened surface in a compressible flow will affect the behavior of a turbulent boundary layer. The flows are simulated using numerical methods and then investigated visually and statistically to reveal the effects of the roughness elements.

II. Methodology

This study is based on a dataset previously simulated and analyzed by Gaskins [19]. Three cases were chosen to analyze, a smooth wall boundary layer case (Case SW), a case with medium roughness height (Case R1), and a case with small roughness height (Case R2). The rough wall is represented by a sinusoidal plane where the no-slip condition is applied. The freestream conditions were chosen from an experiment conducted by Kocher et al. [20]. The flow conditions for the simulations are shown in Table 1. The value of δ_0 is the boundary layer thickness at the inflow plane. The wall temperature was set to be the nominal adiabatic wall temperature for flow of the given Mach number. The Reynolds numbers of the flow can be seen in Table 2. The value of $Re_{\theta i}$ is the incompressible transformation for the momentum thickness Reynolds number given by $Re_{\theta i} = (\mu_\infty/\overline{\mu_w})Re_\theta$ [21].

Table 1 Flow conditions for the numerical simulations.

Parameter	Value
δ_0	5 mm
U_∞	506 m/s
p_∞	26.4 kPa
T_∞	158 K
T_w	266 K
M	2.01
$U_\infty\delta_0/\nu_\infty$	1.364×10^5

Table 2 Reynolds numbers.

Case	k^+	δ^+	$Re_{\theta i}$
SW	0	3800	14,900
R1	182.5	3974	15,600
R2	126.0	3902	15,200

The grids generated are rectangular boxes defined in terms of δ_0. The length, height, and width were respectively set to $100\delta_0$, $6\delta_0$, and $6\delta_0$. The number of grid points in each direction are defined in Table 3. The total number of grid points per grid is approximately 1.4E9. The value of r represents the growth factor of the cell spacing in the wall-normal direction (y). The resolution of the grids can be seen in Table 4. The resolution is sufficient for an implicit large eddy simulation (ILES)[22].

Table 3 Grid sizing.

Case	N_1	N_2	N_3	N	L_1/δ_0	L_2/δ_0	L_3/δ_0	$\Delta y_0/\delta_0$	r
SW	8026	276	626	1.387×10^9	100	6	6	4.5×10^{-4}	1.023
R1	8026	276	626	1.387×10^9	100	6	6	2.0×10^{-4}	1.027
R2	8026	276	626	1.387×10^9	100	6	6	2.0×10^{-4}	1.027

Table 4 Numerical resolution

Case	Δx^+	Δy_w^+	Δz^+	Δy_e^+	$\Delta y_e/\delta$	Δt^+
SW	22.1	0.797	17.1	90.2	0.024	0.300
R1	22.8	0.365	17.7	111.0	0.028	0.312
R2	22.5	0.360	17.4	109.0	0.028	0.311

The rough surfaces were created with a sinusoidal plane. In the rough wall cases, the wall is flat up to $x/\delta_0 = 5.0$. Figure 1 shows a view of the Case R1 grid with magnified views of the roughness elements. The equation which bounds the height of the rough surfaces is

$$y = a \sin\left(2.0\pi \frac{x - x_0}{x_r}\right) \sin\left(2.0\pi \frac{z - z_0}{z_r}\right). \tag{7}$$

In this equation, a is the amplitude of the roughness elements (half the roughness height), x_0 is the streamwise location where the elements start, x_r is the wavelength of the elements in the streamwise direction, and the same definitions apply to the z variables (spanwise direction) with the same subcripts. The values used (defined with respect to δ_0) for the rough grids are $x_0/\delta_0 = 5.0$, $z_0/\delta_0 = 3.0$, $x_r/\delta_0 = 2.5$, $z_r/\delta_0 = 0.5$, $a/\delta_0 = 0.5$ (Case R1), $a/\delta_0 = 0.035$ (Case R2).

The roughness height is twice the amplitude of the roughness elements. It is practical to describe the roughness heights and wavelengths in terms of inner and outer scalings. Table 5 shows the inner and outer-scaled roughness height and wavelength.

Table 5 Roughness parameters.

Case	k/δ	x_r/δ	z_r/δ	k^+	x_r^+	z_r^+
R1	0.046	1.15	0.23	182.5	4563	913
R2	0.032	1.14	0.23	126.0	4500	900

The simulations used a no-slip condition on the lowest surface and the spanwise planes were set as a periodic boundary condition. The top and outlet were set with extrapolation conditions with sponge layers. The inlet boundary condition was set using a similarity solution of the compressible, laminar boundary layer equations [23]. A body force was used to trip the flow to turbulence at $x/\delta_0 = 2.5$. The flow was developed for three flow-through times ($u_\infty T/\delta_0 = 300$) before statistics were collected for an additional minimum of three flow-through times. Three flow-through times equated to 60,000 time steps. Simulations were performed using the DoD's Supercomputing Resource Center (DSRC) cluster Narwhal. The approximate cost for one case to develop and collect statistics is 1.1 million core-hours. The code used for the simulations is the in-house code Wabash which is a higher-order solver of the Navier-Stokes equations [24].

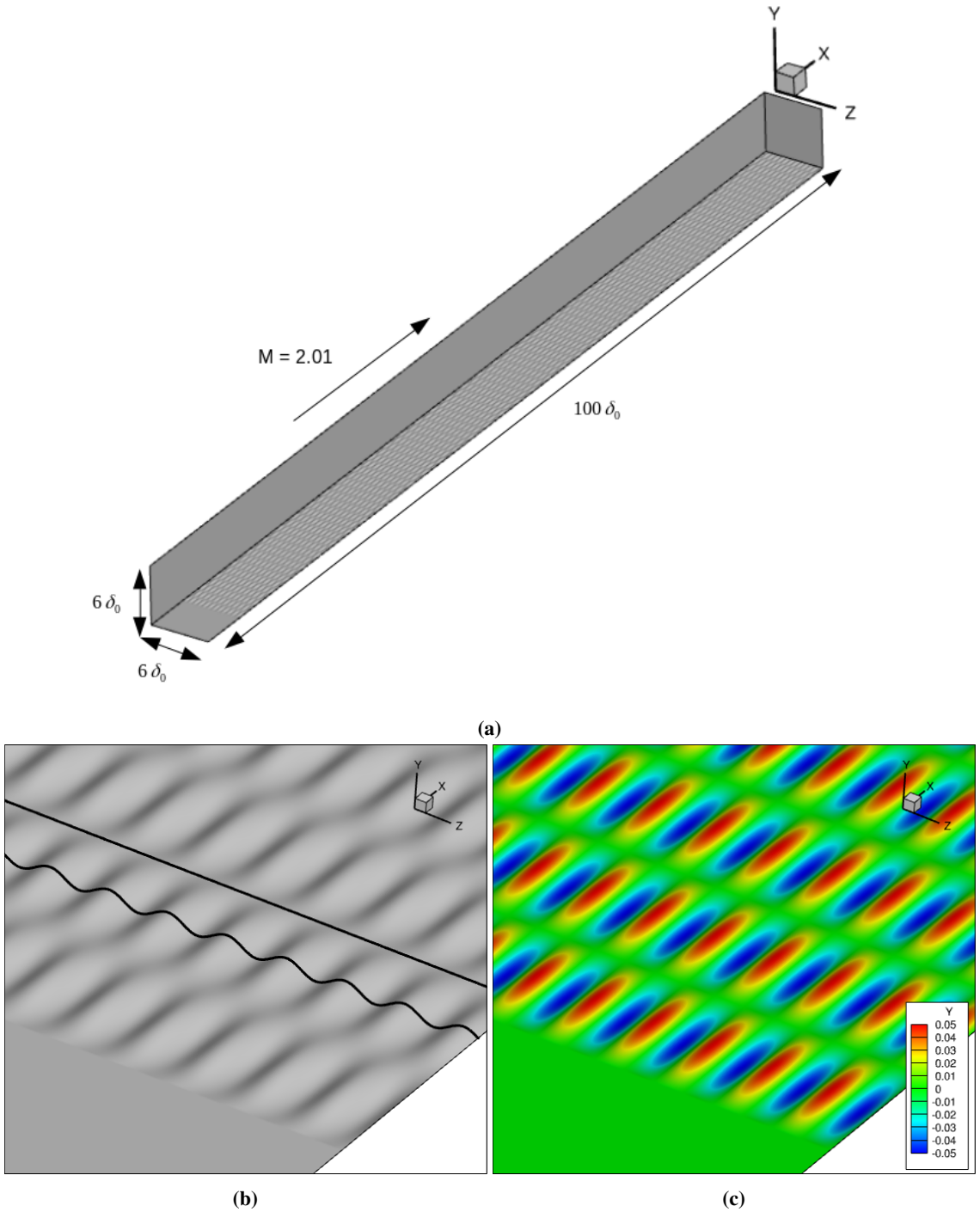

Fig. 1 (a) Isometric view of the Case R1 grid. (b) Magnified view of the roughness elements, shaded with two spanwise lines to aid in visualization of flat and wavy regions across the span. (c) Magnified view of the roughness elements, contour of y.

III. Results

To aid in an understanding of the flowfield, contours of normalized density from the flat wall simulation are displayed in Figure 2. The body force trip can be seen near the start of the computational domain. The flow is seen to trip to turbulence before developing further downstream, seen in the second contour plot. As discussed in a previous study from

Gaskins [19], there are no discernable differences between the large scale flow features between the rough and flat case.

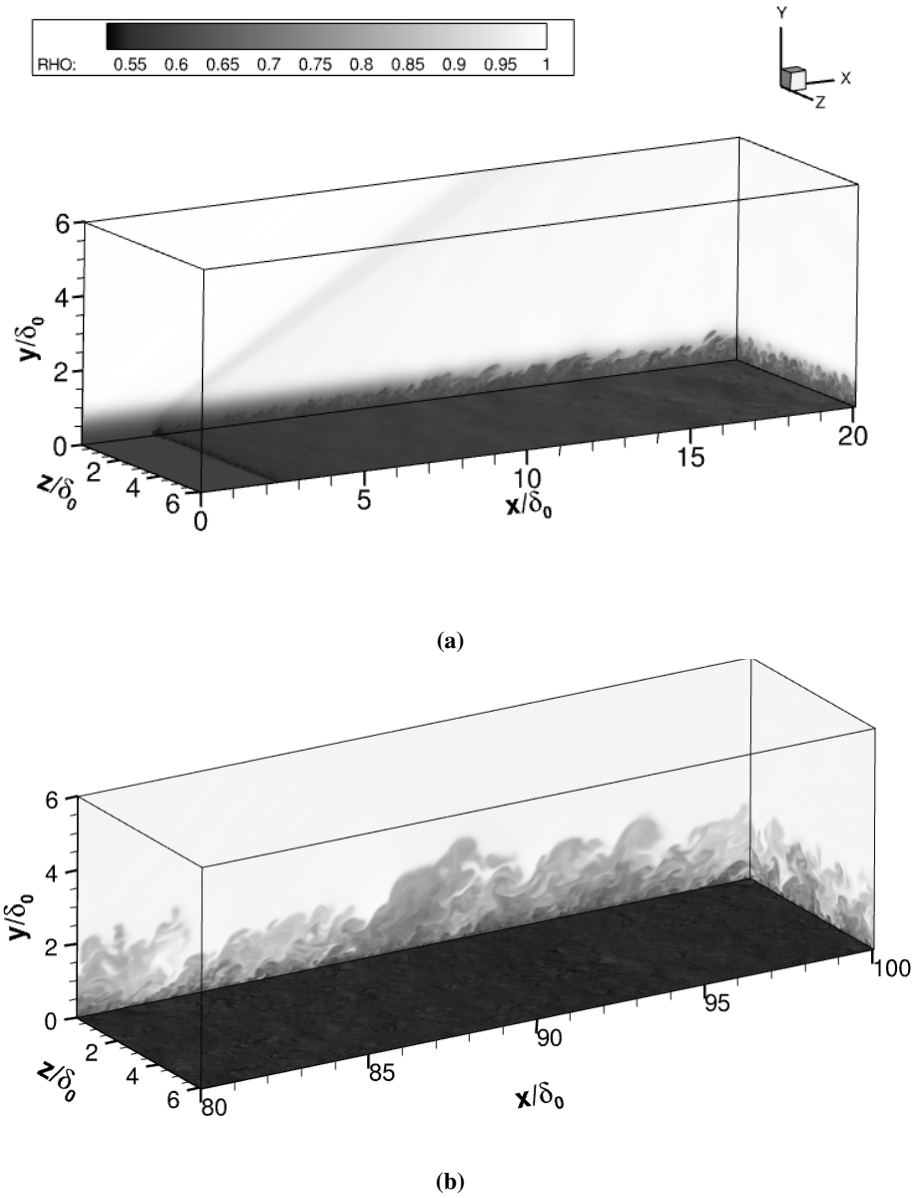

(a)

(b)

Fig. 2 (a) Contour of normalized density at the start of the flat wall case. A Mach wave can be seen at the location of the body force used to trip the flow.(b) Contour of normalized density at the end of the computational domain.

There are some questions as to whether the sinusoidal surface used for the simulations behaves more like a wavy wall or a rough wall. A parameter known as the effective slope is a general guide for determining whether a rough surface is wavy or rough. It is defined as

$$ES = \frac{1}{l_x l_z} \int_0^{l_x} \int_0^{l_z} \left| \frac{\partial k(x,z)}{\partial x} \right| dx dz \tag{8}$$

where l_x and l_z represent the sampled lengths in their subscript's respective directions [1]. A value of the effective slope below 0.35 is considered a wavy surface. The value of the effective slope for Case R1 and Case R2 is 0.051 and 0.036, respectively. This suggests the surface could be considered wavy. To explore this further we can use the value of the coefficient of friction (C_f). A negative value of C_f suggsts that the flow separates, a behavior which may not be typical

of a wavy surface. An investigation of the flowfield has shown that the average value of C_f is positive in all locations. An instantaneous contour of C_f shows there are very limited areas where the value of C_f is negative. This is shown in Figure 3.

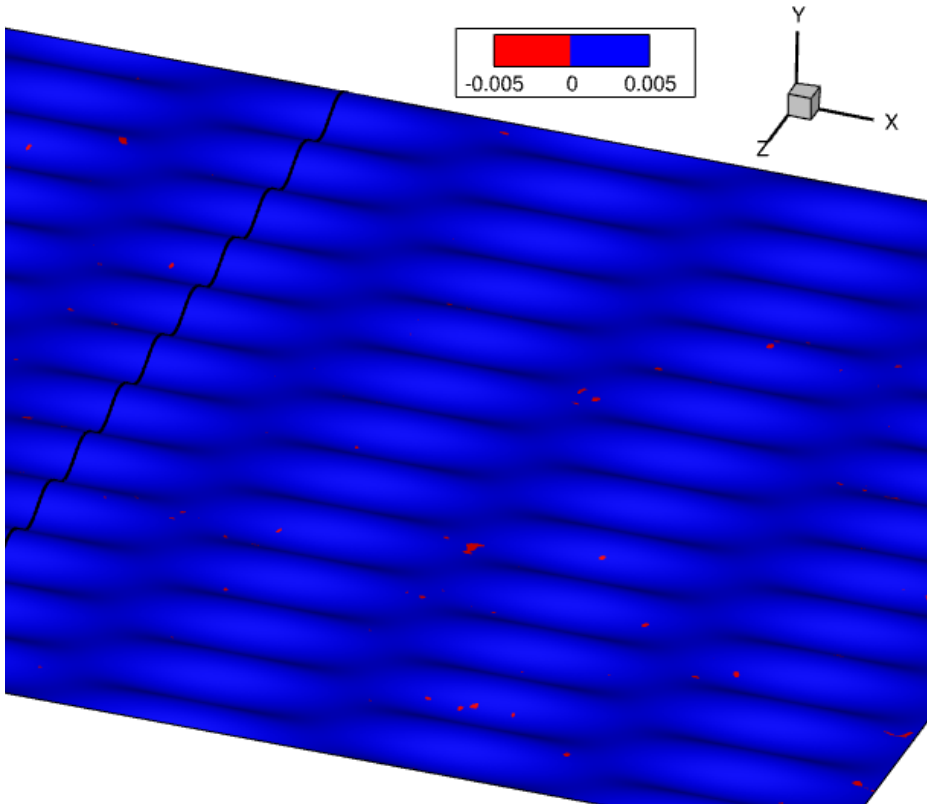

Fig. 3 Instantaneous contour of C_f, with red areas denoting a negative value of C_f. Locations where the flow is separated is very limited.

A coherent structure that has been observed in turbulent boundary layers is near wall streaks of high and low-speed fluid. These streaks are of particular interest in this study, since the disruption of their formation may have an effect on the large scale flow. To investigate these streaks, the normalized values of fluctuating velocites were plotted for Case R1 and Case SW at $y^+ = 18$ (with all wall-normal distances scaled using an effective value of C_f determined at the end of the compuational domain). For Case R1, a plane with constant wall-normal distance was plotted (a sinusoidal plane separated from the wall by a uniform distance with the origin defined as the halfway point between a peak and valley), as the flow is expected to follow the surface after identifying that the values of C_f are positive at all locations on average.

These streaks can be seen for Case SW in Figure 4 and in Case R1 in Figure 5. The streaks in the rough wall case show more coherence and large areas of high speed sweeps. Though the streaks show a different overall pattern, the presence of the streaks is still observed. The spacing of these structures has been shown to be Reynolds number dependent [25], with higher Reynolds number decreasing the spacing between the streaks and increasing the overall number of streaks per unit span. The disturbance of the roughness elements in this case does not appear to be large enough to prevent the formation of the vortices associated with the high and low speed patterns observed here. This may be a physical explanation of Townsend's hypothesis. For high Reynolds number flows, the near-wall streaks become finer and are more resilient to disturbances as they can navigate around the geometric disturbances. This is also consistent with findings that spanwise roughness elements, which completely disrupt the flow near the surface, require higher Reynolds numbers to observe wall-similarity [9].

In video visualizations of the flow, contours of skin friction on the surface and density as the spanwise and streamwise planes were plotted. Frames from the videos can be seen in Figure 6 and Figure 7. Observations of the animated flow have found many interesting features that can be investigated. The presence of the near-wall streaks can be seen in both contours of skin friction from propagation through the shear stress induced from the near-wall velocity. Of particular

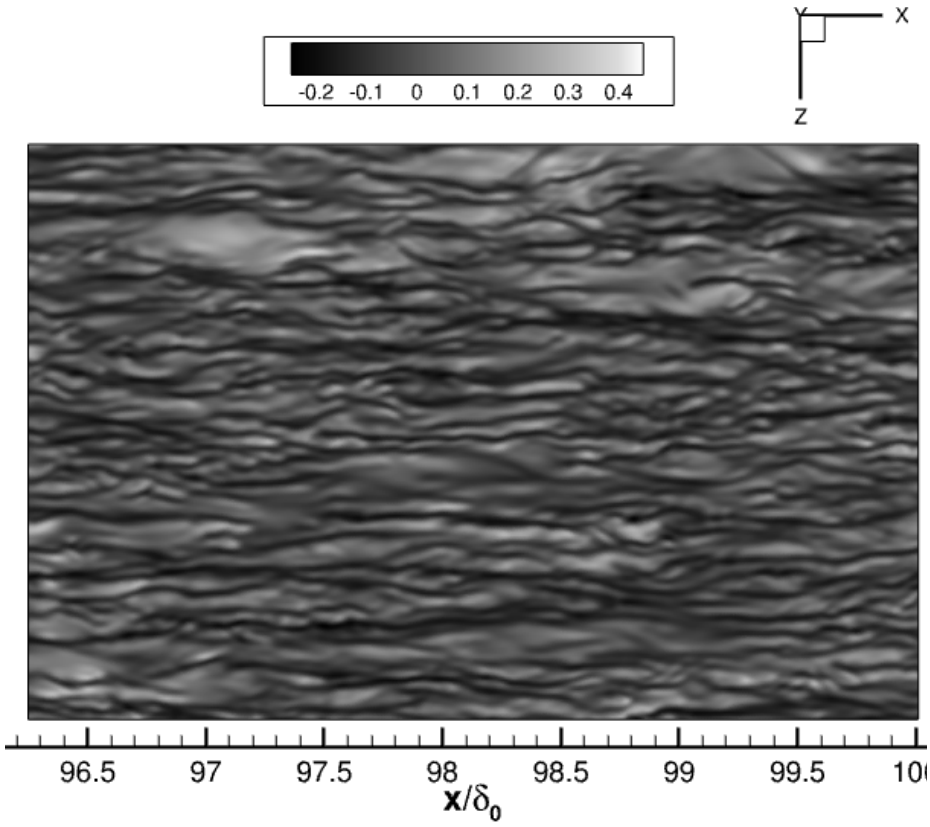

Fig. 4 Streaks of low and high-speed fluid near the wall at $y^+ = 18$, $y/\delta = 0.005$ in Case SW (where δ is the boundary layer thickness at the end of the domain). Contour is of fluctuating velocity normalized by the freestream velocity u'/U_∞.

interest is the large local spots of high C_f in Case R1 which convect downstream. These areas could be related to high local heating from C_f which is of significant interest in high-speed flows. In previous investigations of the flow from Gaskins [19], the regions just past the tip of the roughness elements seemed to be locations where turbulence is produced. The pressure gradients of the surface could act to encourage the production of TKE, and encourage the sweeps of high-speed flow towards the surface, thus potentially causing the increase in C_f.

The production of TKE can be calculated using

$$P = -R_{ij}\overline{u}_{i,j}. \tag{9}$$

The term R_{ij} is a component of the Reynolds stress tensor, and $\overline{u}_{i,j}$ represents the derivative of the mean i velocity component in the j direction. The production of TKE is a scalar, and with the availability of three-dimensional data it is possible to calculate the total production of TKE.

A contour plot of the Morkovin/inner scaled production of TKE was plotted along a peak amplitude line of the roughness elements (Figure 8). In this contour we can see that just after the peak of the roughness element, production is highest. Particularly the production peaks along a horizontal line leaving the peak of the roughness element. As previously stated, the flow is fully attached on average, so this behavior is not from a separated flow. The production term also becomes negative near the valley and on the forward facing portion of the roughness element. Due to the flow being fully attached, this could be expected as the subsonic flow near the surface accelerates and deccelerates in the presence of favorable and adverse pressure gradients, present as a consquence of the geometry. Figure 10 shows a plot of the coefficient of pressure, and is consistent with the previous observations. The regions just after the peaks have adverse pressure gradients, encouraging the production of TKE, and the forward facing portion shows a favorable pressure gradient, decreasing the production of TKE. This is also shown in Figure 9, where the production was integrated in the wall-normal direction along a roughness element. It can be seen that production increases past the peak and goes negative before reaching the next peak.

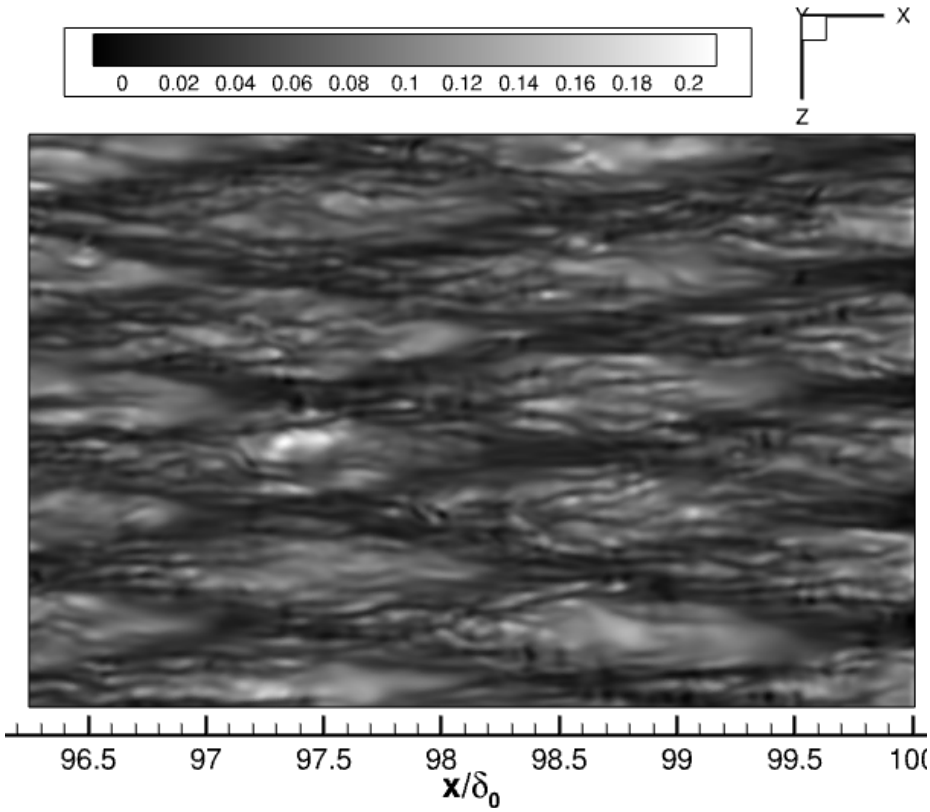

Fig. 5 Streaks of low and high-speed fluid near the wall at $y^+ = 18$, $y/\delta = 0.005$ in Case R1 (where δ is the boundary layer thickness at the end of the domain).

It is worth noting that the roughness elements do not reach past the sonic line of the boundary layer. This flow does not show shock and expansion fans off of the roughness elements that have been observed in several high-speed compressible rough wall studies. The sizing of the roughness elements for this study was initially chosen to have a large value of k^+ with a small value of k/δ. A review paper from Jiménez [26] suggested that for large values of k/δ, the flow in question could be considered "flow around obstacles" and not flow over roughness. A study from Flack and Schultz [9] has suggested that even large values of k/δ could be considered rough wall flows in the limit of high Reynolds numbers flows. Another constraining factor for determing the geometry of the roughness elements was maintaining sufficient resolution between the roughness elements so that the flow could be adequately resolved in these simulations. Rough wall flows with shocks and expansion waves forming around the roughness elements could be a very different flow, and is a topic of interest for a future study. Though this flow does not show shock waves and expansion fans, the behavior of C_f is still shown to be significantly different than Case SW, which is of significant interest in high-speed flow applications.

A. Calculation of the Effective Coefficient of Friction

Determining the value of the coefficient of friction is important for determining value of the friction velocity used for scaling. The coefficient of friciton is related to the friction velocity by

$$C_f = 2(u_\tau/u_\infty)^2. \tag{10}$$

Experimental techniques often use the Clauser chart method [27] to determine the value of C_f, with some modifications for compressible flow. This technique assumes a universal logarithmic region with assumed values of the constants. In the case of this study, additional data is available when performing a high fidelity simulation that allows for the direct calculation of the wall shear stress (and by extension the value of an effective C_f). Here the term "effective C_f" is used to represent the C_f a wall is subjected to if it has roughness but is assumed smooth.

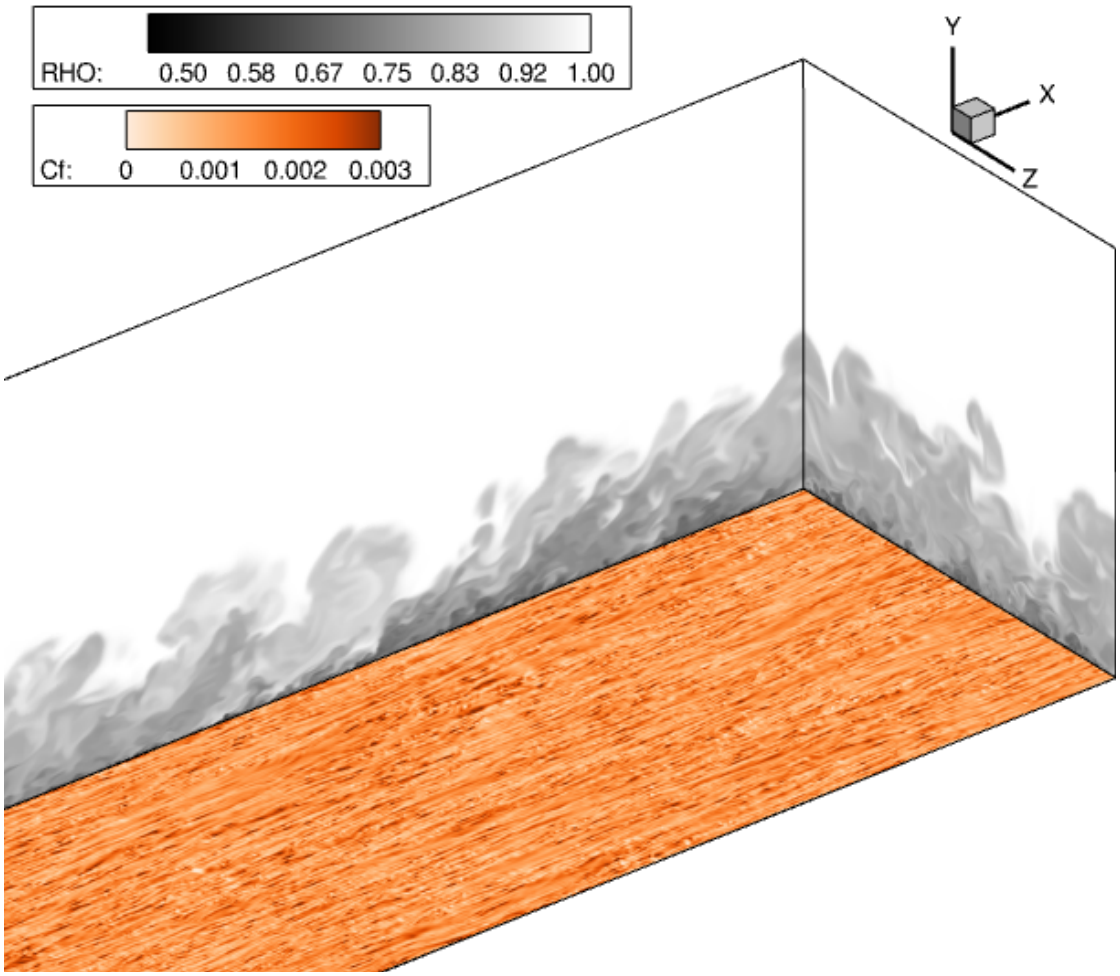

Fig. 6 Isometric view of the smooth wall boundary layer. Contour of skin friction on the surface and density on the spanwise and streamwise planes. Flow is from the bottom left to the top right. Near wall streaks can be seen by extension of the velocity gradients associated with skin friction. Video available at https://engineering.purdue.edu/~jpoggie/rough_wall/flat_cfandrho.mp4.

Thus far, the discussion of C_f involved only the viscous contribution to the wall shear stress. For the smooth wall case, the wall shear stress in the streamwise direction (found to be the dominant component) can be calculated using $\tau_w = \mu \frac{\partial u}{\partial y}$. For the rough wall case, this was not sufficient to calculate the effective wall shear stress, because the orientation of the wall varies and the form drag on the roughness elements was not accounted for. To account for the extra term from form drag, surface unit normal vecotrs derived from grid metrics were used to calculate the surface traction vectors. These vectors were then integrated over a single wavelength of the roughness at the end of the domain in the streamwise direction and over the total span to give a total force per unit wavelength of roughness. The total force per unit length of the surface could then be calculated to determine the value of the effective C_f. This approach is advantageous because it determines the contribution of viscous and form drag on the surface, which is useful for determining the rough flow regime observed. The value of C_{fe} for each case, as well as the contribution of viscous and form drag is seen in Table 6. As previously discussed, the rough flow regime is defined by the effect on the viscous sublayer of the roughness elements. The contribution of the viscous drag is still dominant in the rough wall cases, which would suggest that these cases are most likely transitionally rough. Though the value of k^+ is larger than the value needed for k_s^+ to be in the fully-rough regime, the flow is not fully rough, which suggests that substituting the roughness height as the equivalent sand grain roughness height is not appropriate practice.

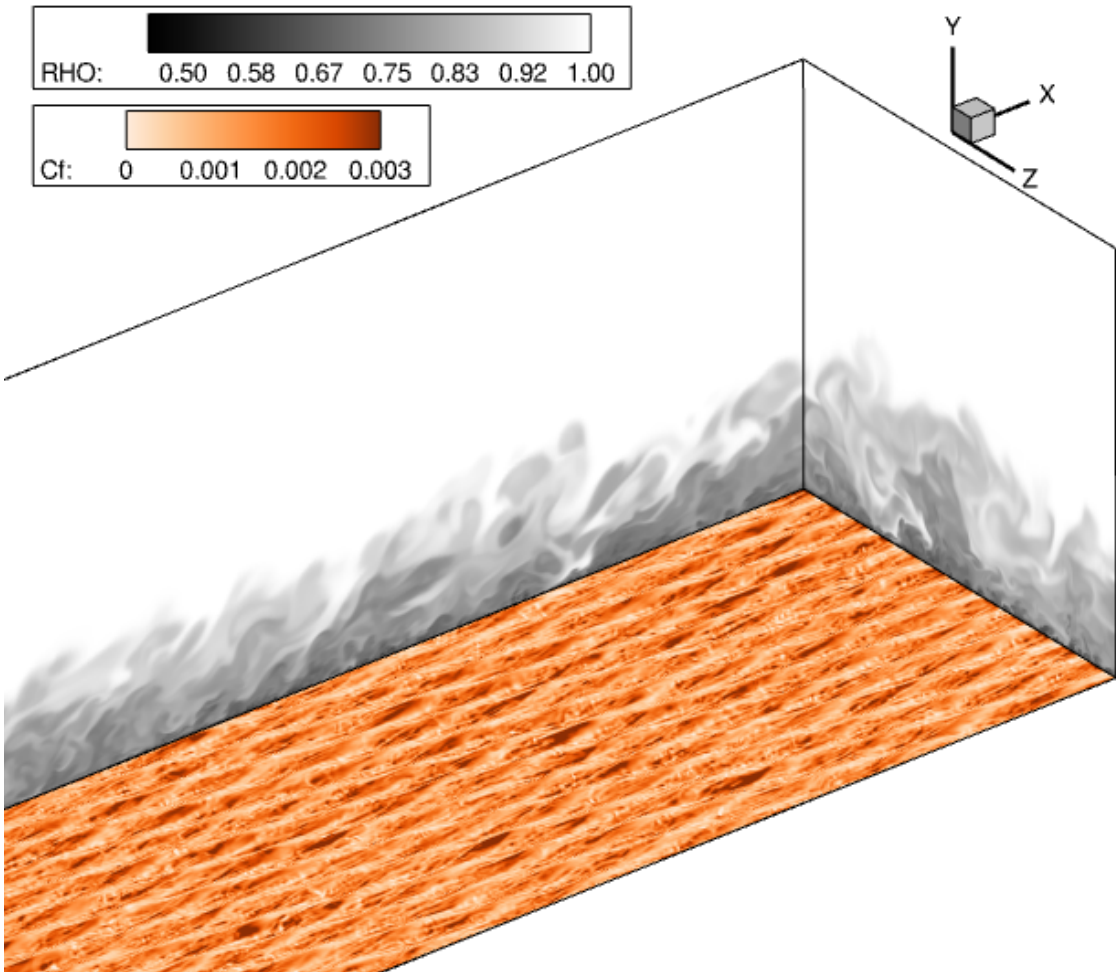

Fig. 7 Isometric view of the Case R1 boundary layer with the same orientation and contours of Figure 6. Video available at https://engineering.purdue.edu/~jpoggie/rough_wall/flat_cfandrho.mp4.

Table 6 Coefficient of friction for the flat and rough wall case

Case	C_f viscous	C_f form	C_{fe}
Smooth Wall	1.376E-3	0.0	1.376E-3
R1	1.356E-3	1.047E-4	1.461E-3
R2	1.371E-3	4.924E-5	1.420E-3

B. Mean Statistics of the Flowfield

With the determination of the effective value of C_{fe}, it is possible to appropriately scale statistics of interest which, in the case of the mean velocity and Reynolds stresses, were collected at a region which is flat across the span at $x/\delta_0 = 98.75$ (with C_{fe} being determined over one wavelength of roughness at the end of the domain). The plane of collected statistics could then be time and spanwise-averaged. The inner-scaled Van Driest transfomed mean velocity profiles can be seen in Figure 11. To investigate for the presence of a logarithmic region, the diagnostic function was plotted in Figure 12 and is given by

$$\Xi = y^+ \left(\frac{\partial u^+_{VD}}{\partial y^+} \right) \tag{11}$$

[25]. A region of constant value would be indicative of logarithmic behavior. For all cases, there is a region which can

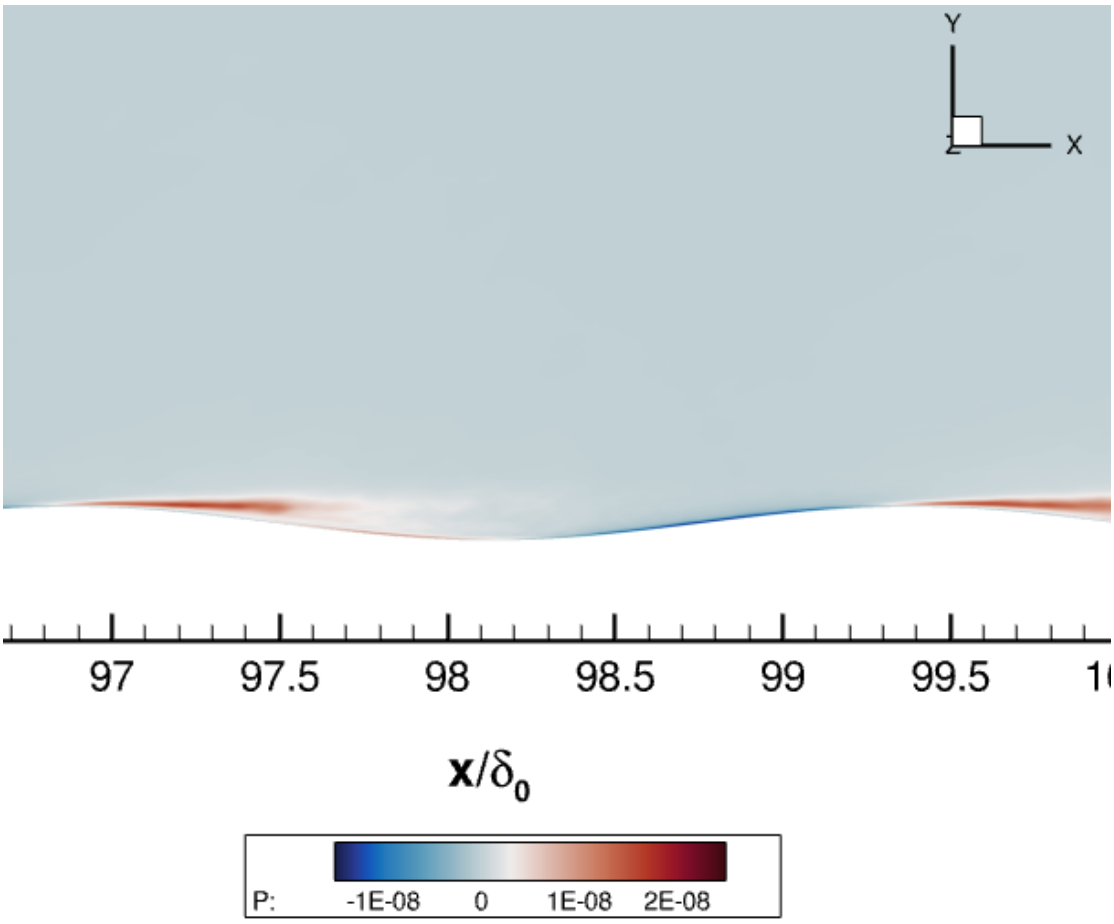

Fig. 8 A contour plot of the Morkovin/inner scaled production of TKE along the highest amplitude region of a roughness element. A region just past the tip of red is a high region of production.

generally be claimed as logarithmic. Estimating the value of the flat region in the diagnostic function determines the value of κ from the log-law. The value of the additive constant B can be determined from curve fitting the logarithmic region in the mean velocity profile. The values of κ and B can be found in Table 7. Case SW and case R2 show a slope near typical values used, but Case R1 shows a significant difference in the slope value. This could be due to disturbances from the rough wall directly affecting the logarithmic region. The direct disturbances of the roughness into the logarithmic region can be observed as a secondary peak in the diagnostic function of Case R1. The secondary peak is consistent with a wall normal location near the top of the roughness elements.

The mean velocity profiles may suggest that this turbulent boundary layer is not yet at an equilibrium state, and is still developing significantly. Ongoing work is involved in incorporating a synthetic turbulence generator as an inflow condition to reduce computational costs of this flowfield and encourage the development of the turbulent boundary layer.

The roughness function is seen as the difference between the rough cases and Case SW (a consequence of increased C_{fe} in the rough wall case). The roughness function is approximately $\Delta u^+ = 1.44$ for Case R1 and 0.62 for Case R2. These values are smaller than what was observed from Kocher et al. [20]. Though the values of k/δ are comparable to the experimental data, the shape of the roughness is different which can have an effect on the behavior of the boundary layer. The values of k^+ is also small compared the the experiments which could also change if the boundary layer was developed further. Kocher et al. observed that the roughness function also develops and increases as a turbulent boundary layer develops. This may also suggest that the turbulent boundary layer is not fully developed.

The Reynolds stresses plotted as functions of outer-scaled y can be seen in Figure 13. A shift in the profiles left of Case SW can be seen in the rough cases. The leftward shift increases with increasing roughness height. This

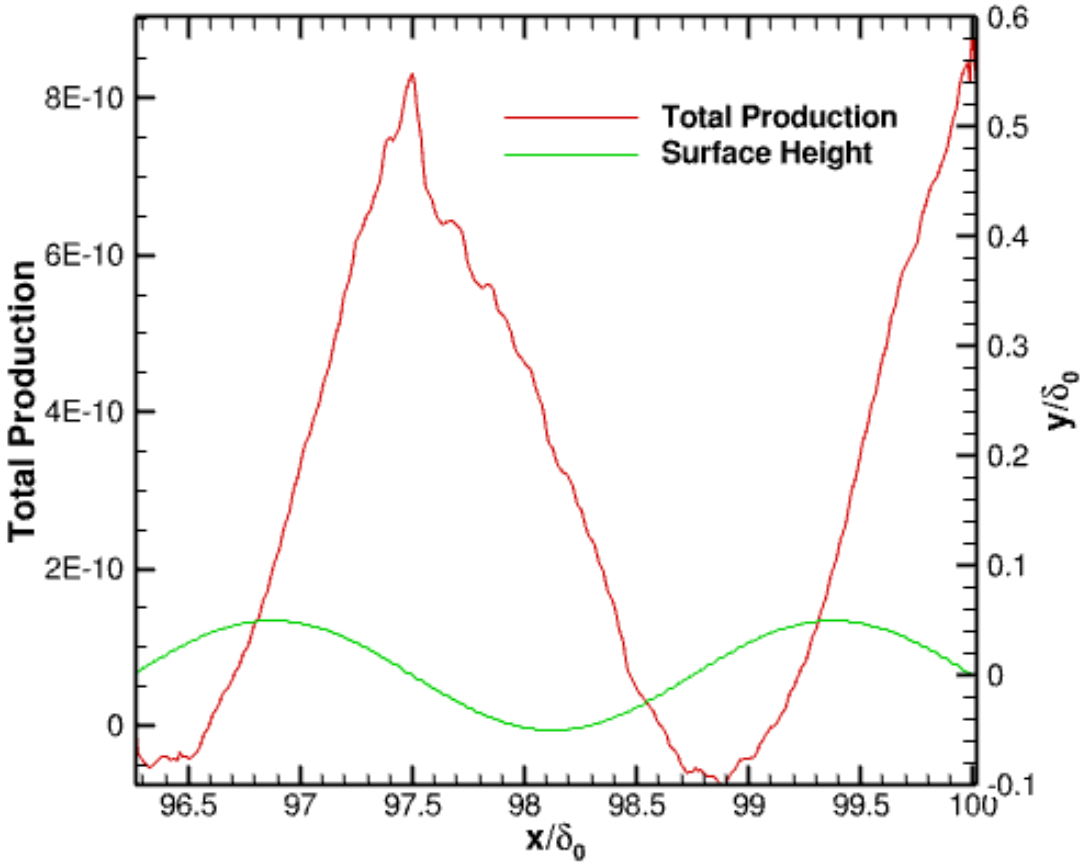

Fig. 9 Wall-normal integrated production of TKE along a roughness element.

Table 7 Log-Law Constants

Case	κ	B
SW	0.392	8.64
R1	0.347	5.29
R2	0.377	7.43
Typical Values Assumed	0.41	5.2

suggests there may be some divergence from wall-similarity when the Reynolds stresses are plotted in this manner, since wall-similarity would show a collapse of the profiles onto each other in the outer region. This may also suggest a need for another scaling parameter or perhaps further investigation into where the effective $y = 0$ point is on the rough surfaces. With the exception of the outer-scaled Reynolds stresses, the inner-scaled Reynolds stresses and mean velocity profiles showed that wall-similarity was present [19].

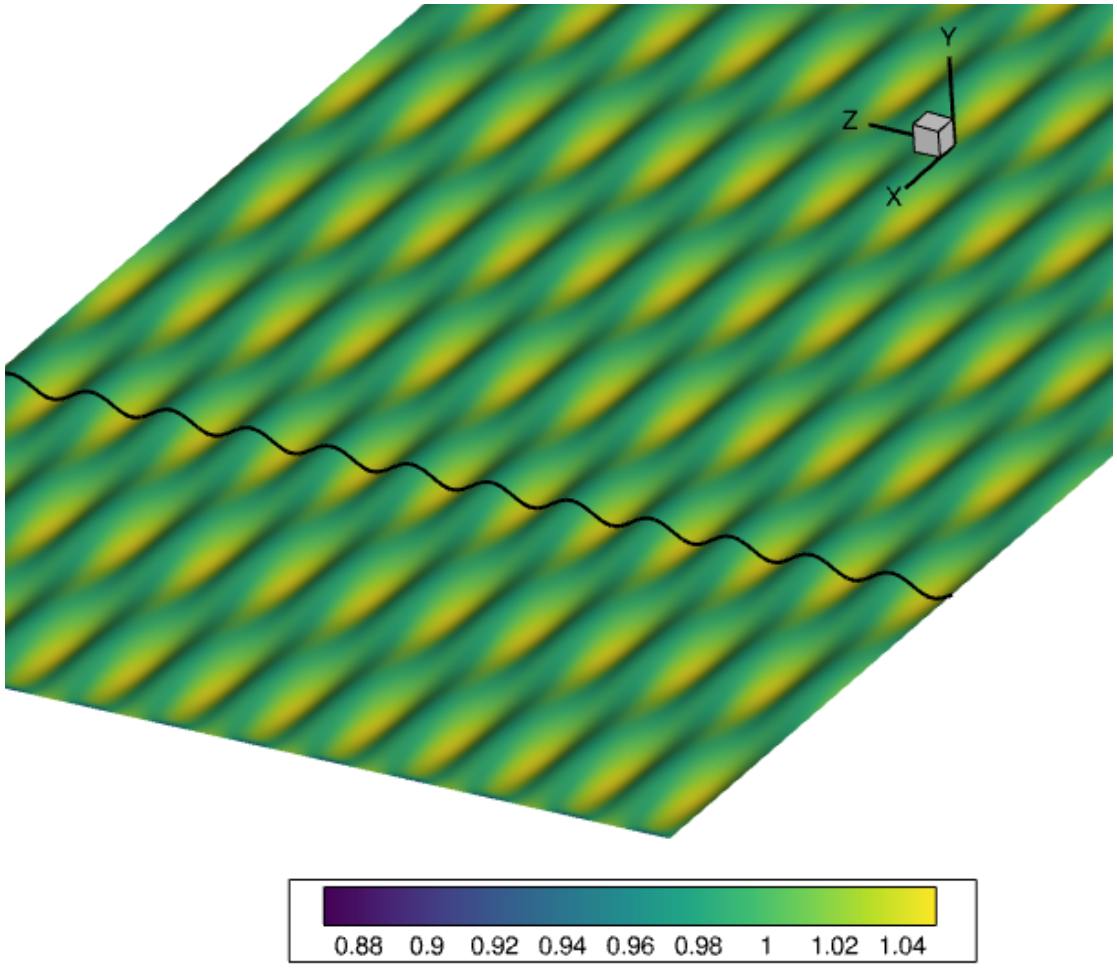

Fig. 10 Coefficient of pressure in Case R1 with a spanwise line to assist visualizing the surface. Pressure gradients can be seen from the high pressure yellow regions to the green lower pressure regions.

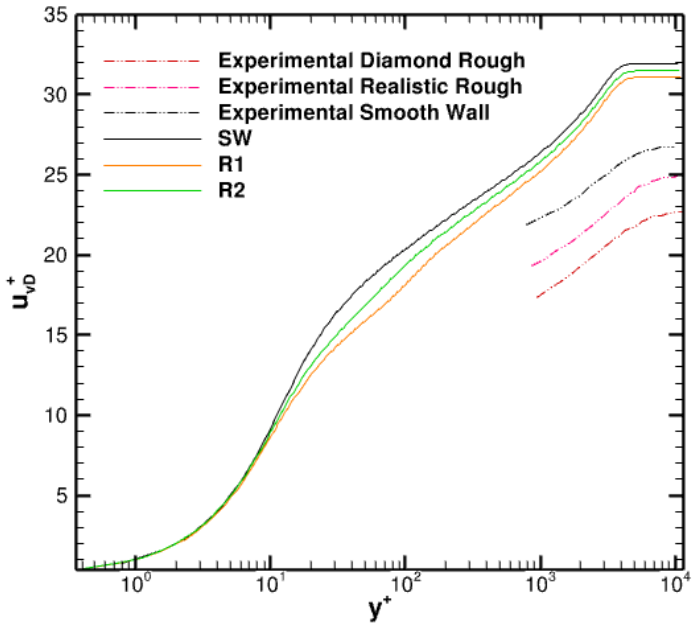

Fig. 11 Van Driest transformed inner scaled mean velocity profiles. The downward shift in rough cases is the roughness function Δu^+.

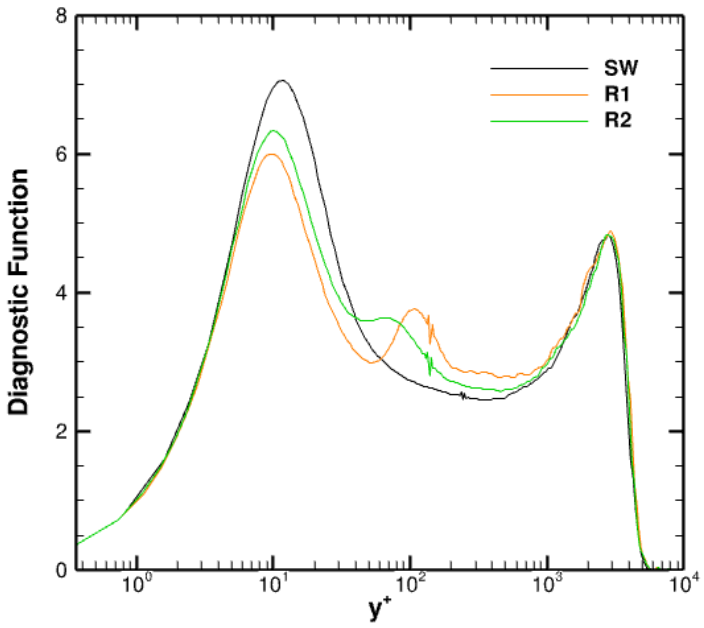

Fig. 12 The diagnostic function (Ξ) value of each of the cases. A constant region would be indicative of logarithmic behavior.

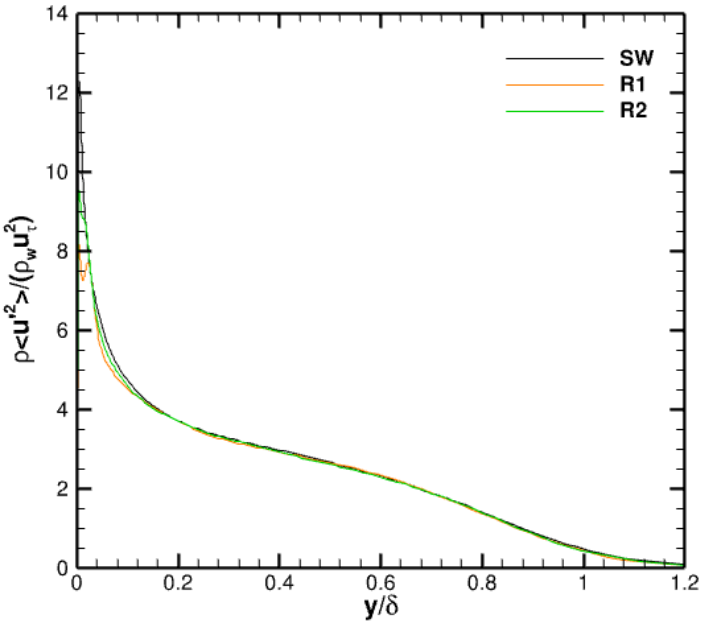
SW
R1
R2
$\rho\langle u''^2\rangle/(\rho_w u_\tau^2)$
y/δ
0
2
4
6
8
10
12
14
0.2
0.4
0.6
0.8
1
1.2

(a)

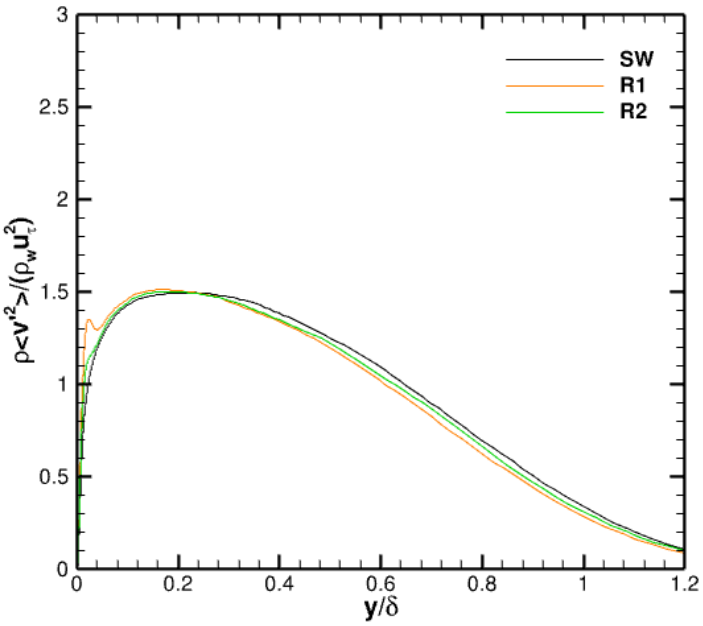
SW
R1
R2
$\rho\langle v''^2\rangle/(\rho_w u_\tau^2)$
y/δ
0
0.5
1
1.5
2
2.5
3
0.2
0.4
0.6
0.8
1
1.2

(b)

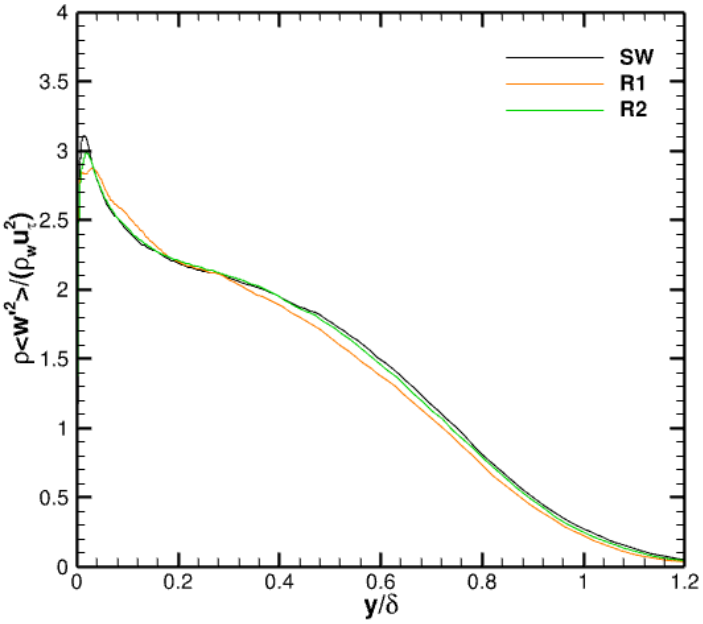

(c)

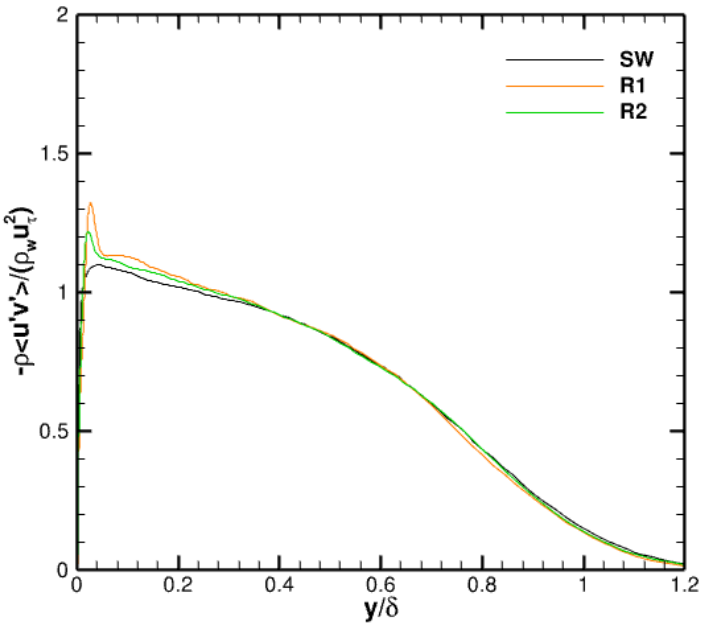

(d)

Fig. 13 The different components of Reynolds stresses shown in inner units using Morkovin scaling as a function of y/δ.

IV. Conclusion

High-fidelity simulations of a relatively high Reynolds number compressible turbulent flow were investigated for a smooth wall case and two rough wall cases of different roughness heights for each case. The behavior of the coefficient of friction near the surface of the cases shows that the rough surface has large local spots of high C_f which convect downstream and are affected by the presence of the roughness elements. An investigation into the production of turbulence kinetic energy shows that just past the tip of the roughness elements is a region of active turbulence producution. The following forward facing portion of the trailing roughness element is a region where production is negative. This is consistent with what is oberved of pressure gradients on the surface.

Coherent high-speed and low-speed streaks near the surface of each case are still observed. They are fine-scale structures due to the high Reynolds number. The streaks are resilient and navigate around the roughness elements, allowing for the development of their associated wall-normal motions. This may be a physical mechanism which explains the Reynolds number similarity hypothesis.

The effective value of the coefficient of friction was calculated directly, which proved useful for determing the regime of rough flow for the rough flow cases. The cases are transitionally rough due to the significance of the viscous drag on the surface in comparison to the smaller contribution of the form drag due to pressure. This may prove to be a useful approach in the future for determining the rough flow regime in numerical studies.

Wall-similarity was observed in all statistics by Gaskins [19] with the exception of the outer-scaled Reynolds stresses. This could be a consequence of needing to determine an effective origin for the roughness elements, or it could suggest that there is a need for another scaling parameter.

The flow appears to still be in a nonequilibrium developing state at the end of the domain. This has encouraged present efforts to incorporate a synthetic turbulence generation inflow condition. Future work also involves investigating a flow where shock waves and expansion fans form around the roughness elements, which could potentially be a significantly different flow.

Acknowledgments

The present work was funded by the Air Force Research Laboratory, under the Multidisciplinary Hypersonics Program. Computer hours were provided by the DoD HPCMP under a Frontier Project. This paper is cleared for public release with case number AFRL-2022-1640.

References

[1] Kadivar, M., Tormey, D., and McGranaghan, G., "A review on turbulent flow over rough surfaces: Fundamentals and theories," *International Journal of Thermofluids*, Vol. 10, 2021, p. 100077. https://doi.org/https://doi.org/10.1016/j.ijft.2021.100077.

[2] Adrian, R. J., "Hairpin vortex organization in wall turbulence," *Physics of Fluids*, Vol. 19, No. 4, 2007, p. 041301. https://doi.org/10.1063/1.2717527.

[3] Van Driest, E. R., "Turbulent Boundary Layer in Compressible Fluids," *Journal of Spacecraft and Rockets*, Vol. 40, No. 6, 2003, pp. 1012–1028. https://doi.org/10.2514/2.7048.

[4] Morkovin, M. V., "Effects of compressibility on turbulent flows." *Mécanique de la turbulence,*, 1962, pp. 367–380.

[5] Zhang, Y.-S., Bi, W.-T., Hussain, F., Li, X.-L., and She, Z.-S., "Mach-Number-Invariant Mean-Velocity Profile of Compressible Turbulent Boundary Layers," *Phys. Rev. Lett.*, Vol. 109, 2012, p. 054502. https://doi.org/10.1103/PhysRevLett.109.054502.

[6] Nikuradse, J., "Laws of flow in rough pipes," , 1950. URL https://ntrs.nasa.gov/citations/19930093938.

[7] Colebrook, C. F., "TURBULENT FLOW IN PIPES, WITH PARTICULAR REFERENCE TO THE TRANSITION REGION BETWEEN THE SMOOTH AND ROUGH PIPE LAWS." *Journal of the Institution of Civil Engineers*, Vol. 11, No. 4, 1939, pp. 133–156. https://doi.org/10.1680/ijoti.1939.13150, URL https://doi.org/10.1680/ijoti.1939.13150.

[8] Moody, L., "Friction factors for pipe flow," *ASME Trans.*, Vol. 66, 1944, pp. 671–684.

[9] Flack, K. A., and Schultz, M. P., "Roughness effects on wall-bounded turbulent flows," *Physics of Fluids*, Vol. 26, No. 10, 2014, p. 101305. https://doi.org/10.1063/1.4896280.

[10] Schultz, M., and Flack, K., "Outer layer similarity in fully rough turbulent boundary layers," *Experiments in Fluids*, Vol. 38, 2005, pp. 328–340.

[11] Lighthill, M. J., "The Structure of Turbulent Shear Flow," *Journal of Fluid Mechanics*, Vol. 1, No. 5, 1956, p. 554–560. https://doi.org/10.1017/S0022112056210366.

[12] Perry, A. E., Henbest, S., and Chong, M. S., "A theoretical and experimental study of wall turbulence," *Journal of Fluid Mechanics*, Vol. 165, 1986, pp. 163–199.

[13] Raupach, M. R., Antonia, R. A., and Rajagopalan, S., "Rough-wall boundary layers," *Applied Mechanics Reviews*, Vol. 44, 1991, pp. 1–25.

[14] Latin, R. M., and Bowersox, R. D. W., "Flow Properties of a Supersonic Turbulent Boundary Layer with Wall Roughness," *AIAA Journal*, Vol. 38, No. 10, 2000, pp. 1804–1821. https://doi.org/10.2514/2.862.

[15] Latin, R. M., and Bowersox, R. D. W., "Temporal Turbulent Flow Structure for Supersonic Rough-Wall Boundary Layers," *AIAA Journal*, Vol. 40, No. 5, 2002, pp. 832–841. https://doi.org/10.2514/2.1749.

[16] Ekoto, I. W., Bowersox, R. D. W., Beutner, T., and Goss, L., "Supersonic Boundary Layers with Periodic Surface Roughness," *AIAA Journal*, Vol. 46, No. 2, 2008, pp. 486–497. https://doi.org/10.2514/1.31729.

[17] Ekoto, I. W., Bowersox, R. D. W., Beutner, T., and Goss, L., "Response of supersonic turbulent boundary layers to local and global mechanical distortions," *Journal of Fluid Mechanics*, Vol. 630, 2009, p. 225–265. https://doi.org/10.1017/S0022112009006752.

[18] Peltier, S. J., Humble, R. A., and Bowersox, R. D. W., "Crosshatch roughness distortions on a hypersonic turbulent boundary layer," *Physics of Fluids*, Vol. 28, No. 4, 2016, p. 045105. https://doi.org/10.1063/1.4944657.

[19] Gaskins, J. J., "The Effect of Near Wall Disturbances on a Compressible Turbulent Boundary Layer," 2021. https://doi.org/10.25394/PGS.16562127.v1, URL https://hammer.purdue.edu/articles/thesis/The_Effect_of_Near_Wall_Disturbances_on_a_Compressible_Turbulent_Boundary_Layer/16562127.

[20] Kocher, B. D., Combs, C. S., Kreth, P. A., and Schmisseur, J. D., *Characterizing the Streamwise Development of Surface Roughness Effects on a Supersonic Boundary Layer*, 2018. https://doi.org/10.2514/6.2018-4047.

[21] Pirozzoli, S., and Bernardini, M., "Probing high-Reynolds-number effects in numerical boundary layers," *Physics of Fluids*, Vol. 25, No. 2, 2013, p. 021704. https://doi.org/10.1063/1.4792164.

[22] Georgiadis, N. J., Rizzetta, D. P., and Fureby, C., "Large-Eddy Simulation: Current Capabilities, Recommended Practices, and Future Research," *AIAA Journal*, Vol. 48, No. 8, 2010, pp. 1772–1784. https://doi.org/10.2514/1.J050232.

[23] White, F. M., *Viscous Fluid Flow*, 2nd ed., McGraw-Hill, New York, 1991.

[24] Poggie, J., Bisek, N. J., and Gosse, R., "Resolution effects in compressible, turbulent boundary layer simulations," *Computers and Fluids*, Vol. 120, 2015, pp. 57–69. https://doi.org/https://doi.org/10.1016/j.compfluid.2015.07.015.

[25] Pirozzoli, S., and Bernardini, M., "Turbulence in supersonic boundary layers at moderate Reynolds number," *Journal of Fluid Mechanics*, Vol. 688, 2011, p. 120–168. https://doi.org/10.1017/jfm.2011.368.

[26] Jiménez, J., "TURBULENT FLOWS OVER ROUGH WALLS," *Annual Review of Fluid Mechanics*, Vol. 36, No. 1, 2004, pp. 173–196. https://doi.org/10.1146/annurev.fluid.36.050802.122103.

[27] Clauser, F. H., "Turbulent Boundary Layers in Adverse Pressure Gradients," *Journal of the Aeronautical Sciences*, Vol. 21, No. 2, 1954, pp. 91–108. https://doi.org/10.2514/8.2938.